forests

MDPI

Article

Investigation of Sound Absorption Properties of Heat-Treated Indonesian Momala (*Homalium foetidum* (Roxb.) Benth.) and Korean Red Toon (*Toona sinensis* (A. Juss.) M. Roem.) Cross Sections

Eun-Suk Jang and Chun-Won Kang *

Department of Housing Environmental Design and Research Institute of Human Ecology, College of Human Ecology, Jeonbuk National University, Jeonju 54896, Korea; esjang@sambosc.com
* Correspondence: kcwon@jbnu.ac.kr

Abstract: This study investigates the effects of heat treatment time and presence of an air back cavity on the sound absorption performance of Indonesian momala (*Homalium foetidum* (Roxb.) Benth.) and Korean red toon (*Toona sinensis* (A. Juss.) M. Roem.) cross sections. To examine the porous characteristics of the two species before and after heat treatment, gas permeability, pore size, and porosity analyses were conducted. Additionally, the sound absorption coefficient was measured based on various heat treatment times and air back cavity sizes. The results showed that, with heat treatment at 210 °C for 6 h, the gas permeability improved by 4.3% for the momala and 38.5% for the red toon, the maximum pore size was improved by 5.25% in the momala and 26.0% in the red toon, and the through-pore porosity improved by 22.7% for the momala and 117.0% for the red toon. Due to these pore structure changes, the noise reduction coefficient (NRC) of the heat-treated momala improved by 6.8%. When a 3-cm air back cavity was applied to the heat-treated momala, the NRC was improved to 92.5%. Similarly, when the same air back cavity was applied to the heat-treated red toon, the NRC was improved to 190.7%. This study demonstrated that an increase in pore size and through-pore porosity by heat treatment triggered an increase in the sound absorption coefficient. Additionally, when an air cavity was applied, the sound absorption coefficient of both heat-treated wood species was increased at low frequency. From the results of this study, we expected that heat-treated momala and red toon cross-sections can be utilized as eco-friendly ceiling materials with sound absorption function.

Keywords: heat treatment; momala; red toon; through-pore porosity; sound absorption coefficient

check for updates

Citation: Jang, E.-S.; Kang, C.-W. Investigation of Sound Absorption Properties of Heat-Treated Indonesian Momala (*Homalium foetidum* (Roxb.) Benth.) and Korean Red Toon (*Toona sinensis* (A. Juss.) M. Roem.) Cross Sections. *Forests* **2021**, *12*, 1447. https://doi.org/10.3390/f12111447

Academic Editor: Angela Lo Monaco

Received: 16 September 2021
Accepted: 22 October 2021
Published: 24 October 2021

Publisher's Note: MDPI stays neutral with regard to jurisdictional claims in published maps and institutional affiliations.

Copyright: © 2021 by the authors. Licensee MDPI, Basel, Switzerland. This article is an open access article distributed under the terms and conditions of the Creative Commons Attribution (CC BY) license (https://creativecommons.org/licenses/by/4.0/).

1. Introduction

Human beings are exposed to high levels of noise on a daily basis, causing the release of the stress hormone cortisol [1] which activates the sympathetic nervous system that raises heart rate, blood pressure, and blood sugar [2]. When this condition persists, even during sleep, stress on the body and the risk of cardiovascular diseases, including angina and arteriosclerosis, increase [1,3].

For this reason, sound absorption and sound insulation are essential features in human-occupied buildings. Synthetic fibers are used traditionally as sound-absorbing materials, but in recent years, "green" sound-absorbing materials have gained research attention due to a growing interest in environmental issues [4–7]. Natural fibers are biodegradable, eco-friendly materials produced from plants, animals, and minerals. For building materials, they usually are fabricated from agricultural wastes and residues composed mainly of cellulose [4–7]. Research on sound-absorbing materials using various types of natural fibers continues to increase, even though (except rice by-products) they are complicated to mass produce.

The Korean Statistical Information Service (KOSIS) reported that world log production has been increasing continuously, from 37.5 million m^3 in 2015 to 39.64 million m^3 in 2019 [8]. Wood can store carbon for an unlimited time until it is burned, and the energy used for manufacturing wood products is low compared to that of other building materials [9]. For these reasons, wood is an eco-friendly material that is sustainable and recyclable and has embodied energy [10].

Wood is an anisotropic material with different properties depending on the anatomical cut surface [11]. Radial and tangential sections of wood have virtually no porosity, which means they can reflect sound; in contrast, cross sections of wood have pores that can absorb sound waves [12]. When sound impinges on a cross section of hardwood, the sound wave penetrates the vessels, converts into thermal energy, and dissipates at the wall of the vessel [12].

The sound absorption performance of hardwood cross sections is correlated with gas permeability [13], and various physicochemical modifications that increase gas permeability have been proposed. These particular wood modifications include heat treatment [14], steam treatment [15], delignification treatment [16,17], sonication treatment [18], and microwave treatment [19]. Heat treatment is the most efficient wood modification to improve sound absorption.

The main purpose of heat treatment is to alter the chemical composition of the wood substance through thermal decomposition to increase its dimensional stability and weather resistance [20,21]. Heat treatment disrupts the cell walls perpendicular to the fiber direction and increases intercellular space [22,23]. This alteration increases the through-pore porosity of heat-treated wood and improves its gas permeability [24,25]. The sound absorption performance of heat-treated wood is greater than that of untreated wood, and the degree of improvement increases as heat-treatment temperature increases [14]. Changes in the physical properties of heat-treated wood differ by species since the wood types possess different chemical compositions. For this reason, the optimal heat-treatment temperature can vary by species [26].

Heat treatment typically is carried out at 200–240 °C [27]. As the temperature increases, thermal decomposition of the wood occurs, accompanied by a decrease in hydrophilicity. This process results in significantly lower hygroscopicity and secures dimensional stability [20]. However, the mechanical performance of wood deteriorates as heat-treatment temperature increases [9,21].

In this study, the heat treatment temperature of 210 °C was selected as it is known to produce high weather resistance against decaying bacteria with only a marginal decrease in strength [27]. Indonesian momala (*Homalium foetidum* (Roxb.) Benth.) and Korean red toon (*Toona sinensis* (A. Juss.) M. Roem.) were selected because they are permeable and readily available. The heat treatment time ranged from 0 to 6 h. An air back cavity of 0 to 3 cm was created because the sound absorption performance of a porous material improves at low frequencies [28–30]. Porosity analysis was conducted based on heat treatment time, and gas permeability and pore size were measured to assess the effects of these changes on sound absorption performance.

2. Materials and Methods

2.1. Sample Preparation

The momala and red toon timbers were prepared by Saehan Timber Co., Ltd. (Goyang-si, Gyeonggi-do, Korea) [17]. Both timbers were taken from the sapwood of trees approximately 30 years old, respectively. They were air-dried, and their original dimensions were 10 cm (R) × 10 cm (T) × 100 cm (L). The timbers were lathed into rods with a 2.9-cm diameter and then cut into 1.0-cm cross sections using a table saw. We selected 11 non-defective (without knots and checking) cylindrical samples of each species. Ten of the cylindrical samples were used to obtain gas permeability, pore size, and sound absorption coefficient, while the remaining one was used to observe the morphology of the vessels. Figure 1

describes the sample manufacturing process, and Table 1 provides the basic physical data of the samples.

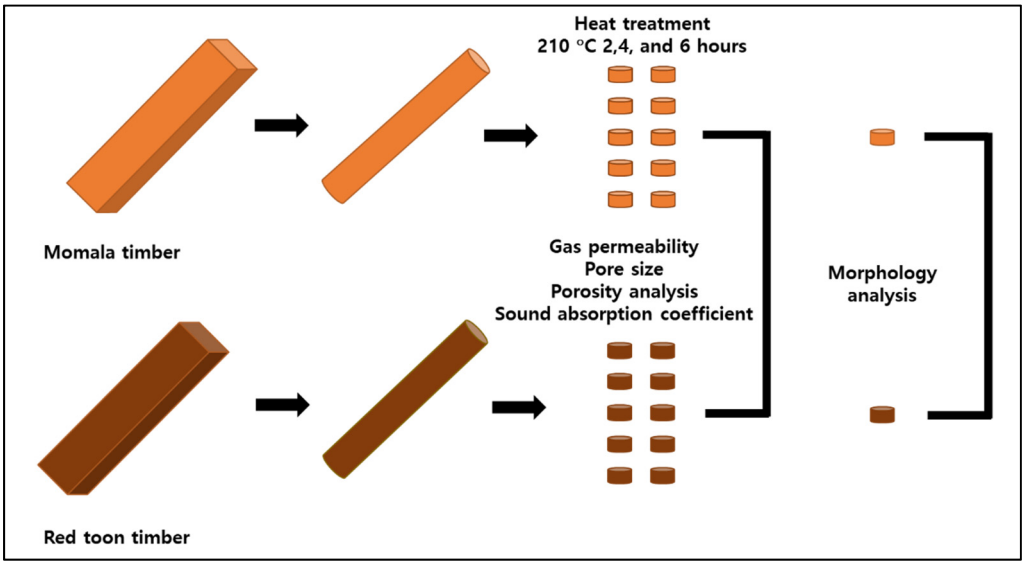

Figure 1. Schematic of sample preparation.

Table 1. Basic physical characteristics of momala and red toon.

Common Name	Scientific Name	Origin	Type *	Mass (g)	Air-Dried Density (g/cm^3)	Porosity (%)	MC (%)
Momala	*Homalium foetidum* (Roxb.) Benth.	Indonesia	Dp	5.17 ± 0.10	0.80 ± 0.02	46.79 ± 1.09	7.5
Red toon	*Toona sinensis* (A. Juss.) M. Roem.	Korea	Rp	3.69 ± 0.08	0.57 ± 0.01	61.80 ± 0.08	7.5

* Dp, diffuse-porous wood; Rp, ring-porous wood.

2.2. Heat Treatment

The heat treatment was performed at 210 °C for 6 h using a laboratory air dryer (OF-02GW; Jeotech Co., Ltd, Daejeon, Korea). The heat-treated samples were placed in the laboratory (20 °C and 50% humidity) for 1 h before morphology analysis, gas permeability, pore size, and porosity analysis and sound absorption coefficient measurements. The sound absorption coefficient was measured in the samples every 2 h after heat treatment. Morphology analysis, gas permeability, pore size, and porosity analysis were conducted before and after heat treatment for 6 h.

2.3. Scanning Electron Microscopy (SEM) Analysis

The SEM (Genesis-1000; EmCrafts Co., Ltd., Sungnam, Korea) was used to observe the changes in wood morphology before and after heat treatment. The specimens were pretreated by softening and drying before SEM measurement [25,31]. The cross sections and radial sections of each species were observed at 200×.

2.4. Gas Permeability

A capillary flow porometer (CFP-1200AEL; Porous Materials Inc. (PMI), Ithaca, NY, USA) was used to measure permeability in the fiber direction as it changed with heat treatment time. As the air pressure was increased from 0 to 1 bar, the flow rate was measured

according to pressure. The Darcy permeability constant was calculated automatically by the CFP-1200AEL's software (Capwin v. 6.74.110), using Equation (1) [25,31]:

$$C = 8FTV_a/\pi D^2\left(P^2 - 1\right) \quad (1)$$

where C = Darcy permeability constant; F = flow; T = sample thickness; V_a = viscosity of air; D = sample diameter; and P = pressure.

2.5. Pore Size Analysis

Pore size was measured by capillary flow porometry [32–34] using the standard method of ASTM F-316 [35]. This method's main characteristic is that it measures the constricted segments of only the through-pores to measure only the pores that affect permeability [25,31,34–39]. The same equipment used for gas permeability was used to measure pore size.

2.6. Porosity Analysis

Figure 2 shows the classification of solid porous materials. The International Union of Pure and Applied Chemistry (IUPAC) stated in their 1994 publication Recommendations for the Characterization of Porous Solids (Technical Report) [40] that the physical pore shape of a solid porous material is classified into three types: through-pores with both ends open, blind pores with one end open, and closed pores without communication to the outside of the material. The combination of a through-pore and a blind pore is called an open pore.

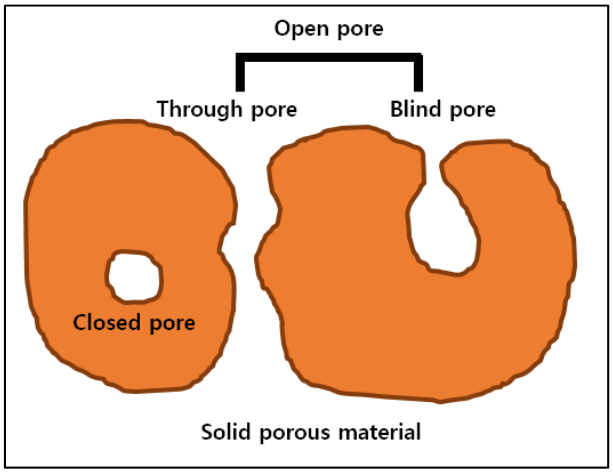

Figure 2. Classification according to the pore shape of a solid porous material.

The open-pore porosity of solid porous materials can be obtained using gas pycnometry [41–43]; we used model PYC-100A-1 from PMI, Inc. according to ISO 12154 [44] to assess the open pores of the cylindrical samples. We calculated the closed-pore porosity (ϕ_{closed}) as the difference between total porosity (ϕ_{total}) and the open-pore porosity (ϕ_{open}) using Equation (2):

$$\phi_{\text{closed}}\ (\%) = \phi_{\text{total}} - \phi_{\text{open}} \quad (2)$$

Our separation of open-pore porosity into through-pore porosity and blind-pore porosity was consistent with previous studies [17,25,31,38]. First, we weighed the dried samples. Next, we immersed each sample in Galwick® (PMI, Inc., Ithaca, NY, USA) solution and subjected it to vacuum for 15 min in a vacuum chamber. The solution easily penetrated into the sample's open pores since it had a particularly low surface tension (0.159 mN/m). This solution also has a high specific gravity (1.79) and extremely low volatility (0.025 torr at 20 °C) and is suitable for porosity analysis

Each sufficiently wetted sample was placed in the chamber of the CFP. Air pressure was applied in the longitudinal direction, and the solution inside the through-pores escaped. Then we weighed the sample again and calculated the blind-pore porosity based on the difference between this weight and the original dried weight, using Equation (3):

$$\phi_{\text{blind}}\ (\%) = \left(\frac{(m_1 - m_0)/1.79}{V} \right) \times 100 \quad (3)$$

where m_0 = sample mass before wetting, m_1 = sample mass after Galwick® extrusion, and V = sample volume.

The through-pore porosity was calculated by Equation (4):

$$\phi_{\text{through}}\ (\%) = \phi_{\text{open}} - \phi_{\text{blind}} \quad (4)$$

2.7. X-ray Diffractometer (XRD) Analysis

Lignin and Hemicellulose are amorphous. However, cellulose has amorphous and crystalline regions. In this study, a high-performance XRD (model: G8 Advance, Bruker, Germany) was used to compare cellulose crystallinity of specimens before and after heat treatment. XRD is the most widely used analytical technique to investigate the crystallinity and crystallite size of wood materials [45]. A wooden specimen sliced through a radial section was examined by X-ray at a scan range of XRD of 2θ = 5°–80°, step width of 0.025, and a scan speed of 5°/min [15]. In the XRD pattern, crystalline appears as a peak at a specific location. The area of crystalline peaks and the area of all peaks, including crystalline and amorphous, were calculated from these peaks. In this study, the XRD software (Diffrac. EVA Ver 6.0) automatically calculated the crystallinity value.

2.8. Sound Absorption Analysis

The transfer function method according to ISO 10534-2 [46] is useful to measure the sound absorption properties of small samples at the laboratory scale. We measured the sound absorption coefficient of the cylindrical samples at a frequency band of 50–6400 Hz using an impedance tube (Type 4236; Brüel & Kjær, Nærum, Denmark). Then we calculated the noise reduction coefficient (NRC), which in this case was the average of the sound absorption coefficients at 250, 500, 1000, and 2500 Hz. We also calculated the average sound absorption coefficients at the 250–500 Hz, 500–1000 Hz, 1000–2000 Hz, and 2000–6400 Hz frequency bands.

To further investigate the effect of the air back cavity, the sound absorption coefficient was measured while adjusting the air back cavity to 1 cm, 2 cm, and 3 cm at the rear of the sample. When the air back cavity was applied, we inserted O-rings at the front and back of the sample to prevent experimental errors due to the air gap between the sample and the inner wall of the impedance tube [16].

2.9. Statistical Analysis

Paired *t*-tests were conducted to determine the differences between the mean of gas permeability, pore size, porosity, and NRC before and after heat treatment. Multiple regression analysis was performed to investigate how heat treatment time and air back cavity affected NRC. The enter method was estimation of the regression equation used in this study, which analyzed all independent variables under consideration here. The influence of a specific independent variable can be determined while the other independent variables are controlled, and the degree to which all independent variables that simultaneously explain the dependent variable can be identified [47]. Equation (5) shows the multiple regression model:

$$Y = \alpha_0 + \beta_{1\times1} + \beta_2\ X_2 + \beta_3\ D_1 + \varepsilon \quad (5)$$

where Y is the NRC, X_1 is the treatment time, X_2 is the air back cavity size, D_1 is the wood dummy variable (1 if the wood is red toon, otherwise 0), α_0 is the constant (intercept term), and ε is the residual (error term).

3. Results and Discussion

3.1. SEM Images of Momala and Red Toon

Figure 3 provides SEM images of momala and red toon before and after heat treatment. Momala is a diffuse-porous wood, and its vessels are distributed evenly over a wide area, whereas red toon is a ring-porous wood with large vessels in its spring wood. The vessels become smaller with the progression into summer wood. Significant macroscopic anatomical changes in momala were not observed after heat treatment [24]; however, red toon developed microcracks inside the vessels after heat treatment.

3.2. Gas Permeability Pore Size and Porosity Analysis

Figure 4 provides the variations of gas permeability, pore size, and porosity in both wood species. The gas permeability of momala prior to heat treatment was 12.2 Darcy, which increased approximately 4.3% to 12.7 Darcy ($t = -1.995$, $p < 0.10$, paired t-test) after heat treatment (210 °C for 6 h). The gas permeability of red toon prior to heat treatment was 6.742 Darcy, which increased by approximately 38.5% to 9.3 Darcy ($t = -7.949$, $p < 0.01$) after heat treatment.

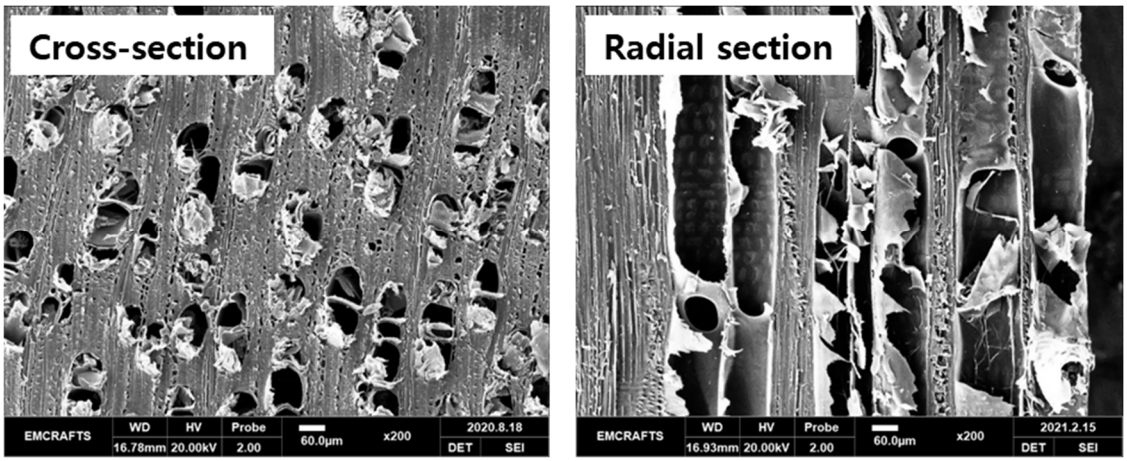

(**a**)

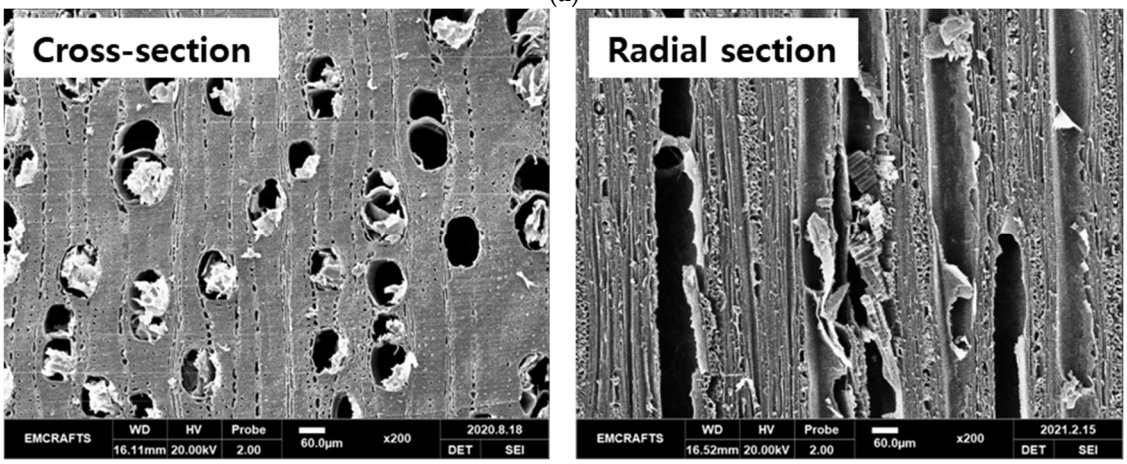

(**b**)

Figure 3. *Cont.*

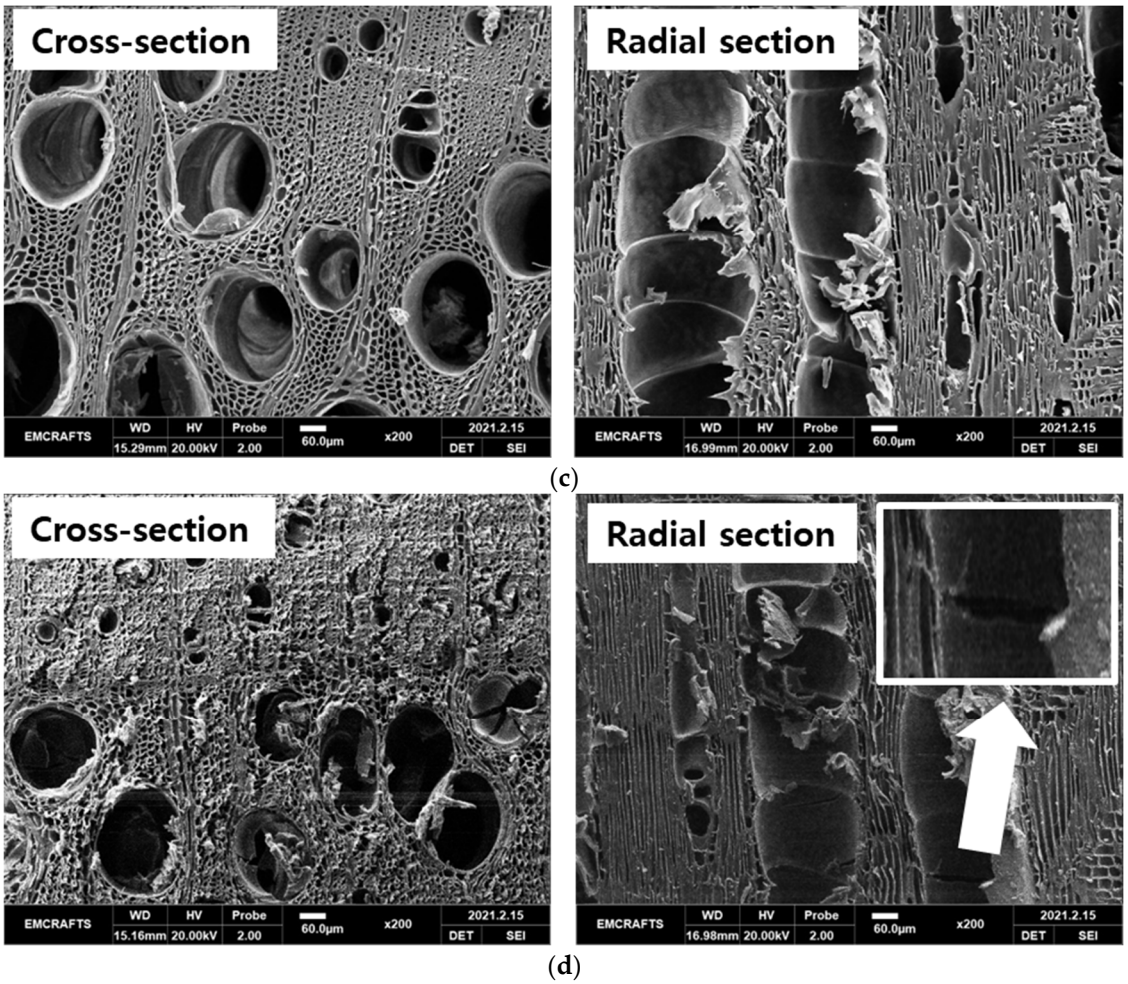

Figure 3. SEM images of momala and red toon before and after heat treatment. (**a**) Before treatment of momala, (**b**) after treatment of momala, (**c**) before treatment of red toon, (**b**) after treatment of red toon.

The maximum pore size of momala prior to heat treatment was 53.4 ± 2.7 μm, which increased by approximately 5.2% to 56.1 ± 2.4 μm ($t = -2.420$, $p < 0.05$) after heat treatment; the difference in mean pore size ($t = 0.158$, $p = 0.878$) was not significant. The maximum pore size of red toon prior to heat treatment was 128.2 ± 19.3 μm, which then increased by approximately 26.0% to 161.5 ± 19.5 μm ($t = -4.556$, $p < 0.001$) after heat treatment; the difference in mean pore size ($t = 0.512$, $p = 0.620$) was not significant.

The weight and density of momala before heat treatment were 5.17 ± 0.10 g and 0.80 ± 0.02 g/cm^3, respectively, and after heat treatment, they were 4.75 ± 0.10 g and 0.82 ± 0.02 g/cm^3, respectively. The weight and density of red toon before heat treatment were 3.69 ± 0.08 g and 0.57 ± 0.01 g/cm^3, respectively, and after heat treatment, they were 3.31 ± 0.07 g and 0.54 ± 0.01 g/cm^3, respectively. The environmental conditions were a temperature of 20 C and 50% humidity. Accordingly, after heat treatment, the total porosity of momala decreased by about 2.7% from 46.78 ± 1.31% to 45.50 ± 1.24% ($t = 2.396$, $p < 0.05$). Additionally, that of red toon increased about 3.5% from 61.81 ± 0.80% to 63.99 ± 0.73% ($t = -34.963$, $p < 0.001$). At least in this experimental result, the change in total porosity by heat treatment was insignificant. The reason is that the weight decreased after heat treatment, but the specimen shrinks, and the volume is reduced. However, the through-pore porosity of momala prior to heat treatment was 23.7 ± 1.0%, which increased by approximately 22.7% to 29.1 ± 1.485% ($t = -9.151$, $p < 0.001$) after heat treatment. The through-pore porosity of red toon prior to heat treatment was 13.0 ± 1.9%, which increased by approximately 117.0% to 28.3 ± 4.3% ($t = -12.023$, $p < 0.001$) after heat treatment.

Pore structure did not change significantly in the macroscopic SEM images of momala after heat treatment. Typically, hemicellulose was decomposed in the heat-treated wood, and the degree of crystallinity changes [21]. The chemical change of wood through heat treatment causes mass reduction [23], and this can convert the pore structure of the wood into a permeable structure [22]; this suggests that, in theory, heat may increase momala maximum pore size and through-pore porosity. That is, through heat treatment of momala, the pore structure can be altered in the direction of increasing through-pore porosity, leading to improvement of gas permeability.

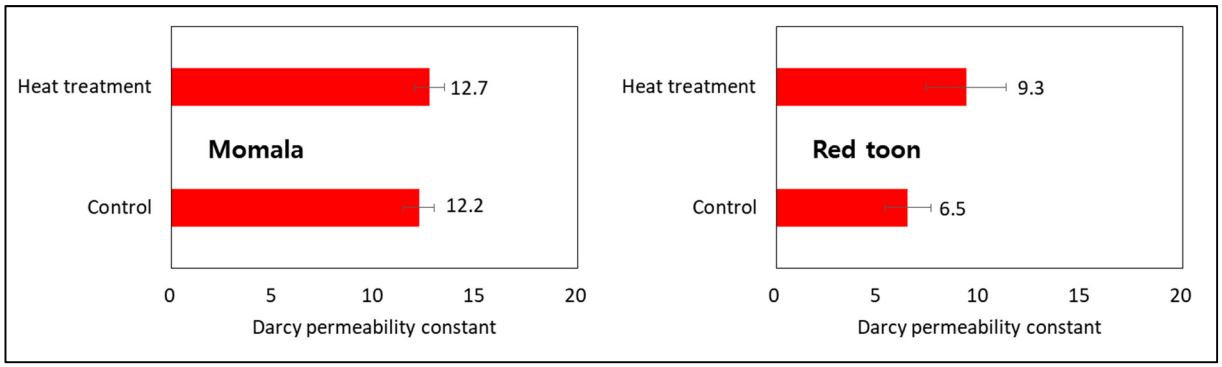

(**a**)

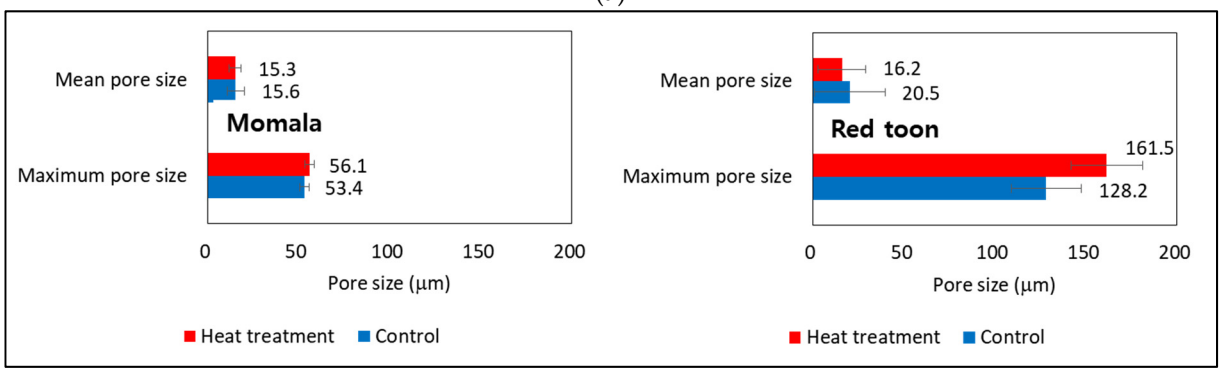

(**b**)

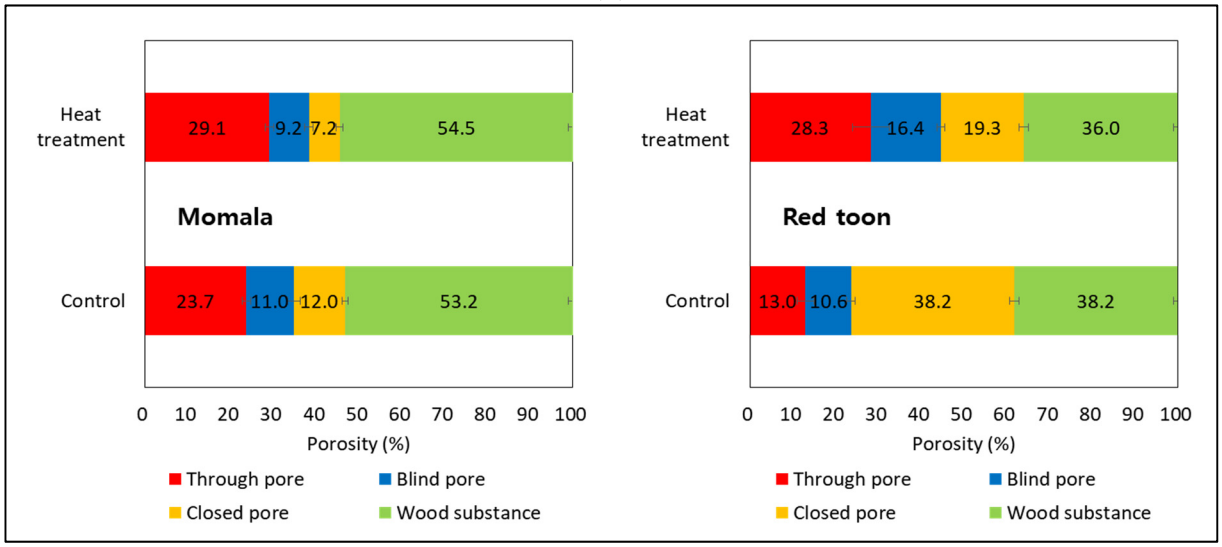

(**c**)

Figure 4. Results of gas permeability (**a**), pore size (**b**), and porosity analysis (**c**) before and after heat treatment of momala and red toon.

As mentioned, microcracks in the vessels were observed in red toon. For this reason, the increases in pore size and through-pore porosity were greater than those of momala, and they also affected its increase in gas permeability. Consequently, the gas permeability of red toon improved due to increases in maximum pore size and through-pore porosity and the development of microcracks after heat treatment.

3.3. XRD Analysis

Figure 5 illustrated the XRD analysis of momala and red toon before and after heat treatment. The peaks at 16.0, 22.6, and 24.4 for untreated momala are transferred to 15.8, 22.3, and 22.4 in heat-treated momala sample. Additionally, the peaks at 16.1 and 22.0 for un-treated red toon are transferred to 16.2 and 22.3 in heat-treated red toon. The cellulose crystallinity is found to be 51.0% for untreated momala and 36.9% for heat-treated momala, while 52.2% for untreated red toon and 37.8% for heat-treated red toon.

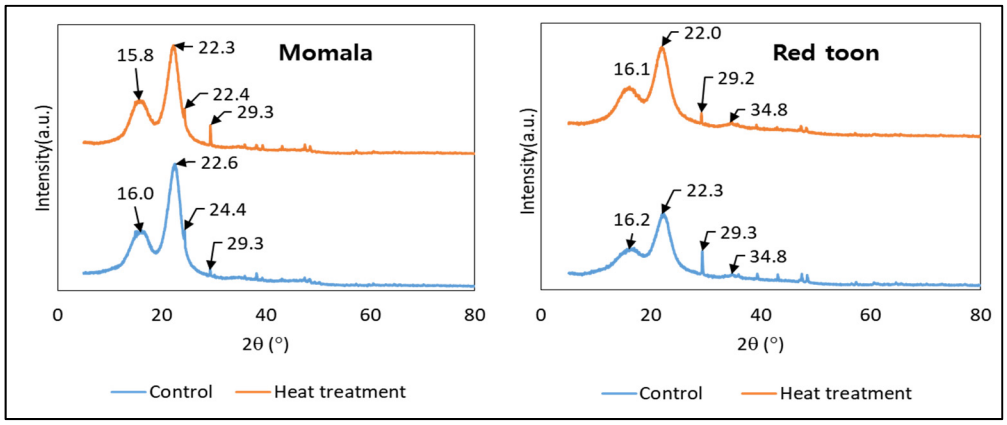

Figure 5. XRD analysis of momala and red toon before and after heat treatment.

These results suggest a slight change in the cell wall and cellulose crystallinity of the heat-treated wood. This chemically modified wood cell wall can help to improve through-pore porosity and improved sound absorption performance.

3.4. Sound Absorption Properties

Figure 6 illustrates the sound absorption curves of momala and red toon before and after heat treatment with air back cavities of different sizes. Table 2 provides the NRC and average sound absorption coefficient values at 250–500 Hz ($\alpha_{250–500}$), 500–1000 Hz ($\alpha_{500–1000}$), 1000–2000 Hz ($\alpha_{1000–2000}$), and 2000–6400 Hz ($\alpha_{2000–6400}$).

The trend of momala sound absorption curve showed that the sound absorption coefficient was low in the low-frequency band and increased as the frequency band increased. The low-frequency band sound absorption coefficient, however, improved when an air back cavity was applied. This is a typical characteristic of porous sound absorbers, as shown in previous studies [48–51]. Overall, as the heat treatment time of momala increased, the sound absorption coefficient also increased. In particular, the sound absorption coefficient rate at 2000–6400 Hz increased significantly by 5.0% ($t = -2.062$, $p < 0.1$) during the 6-hour heat treatment.

As to the effect of improving sound absorption performance through heat treatment, the sound absorption coefficient of 2000 Hz or less increased as the size of the air cavity increased. This improved momala NRC. The NRC of the untreated momala was 0.147 ± 0.005, and after heat treatment for 6 h, the NRC was increased by 6.8% to 0.157 ± 0.012 ($t = -2.089$, $p < 0.1$). When a 3-cm air cavity was applied, the NRC was 0.283 ± 0.021, a 92.5% increase ($t = -18.083$, $p < 0.001$) compared with the untreated momala. Based on these findings, we determined that the overall momala sound absorption performance could be significantly improved by applying an air cavity.

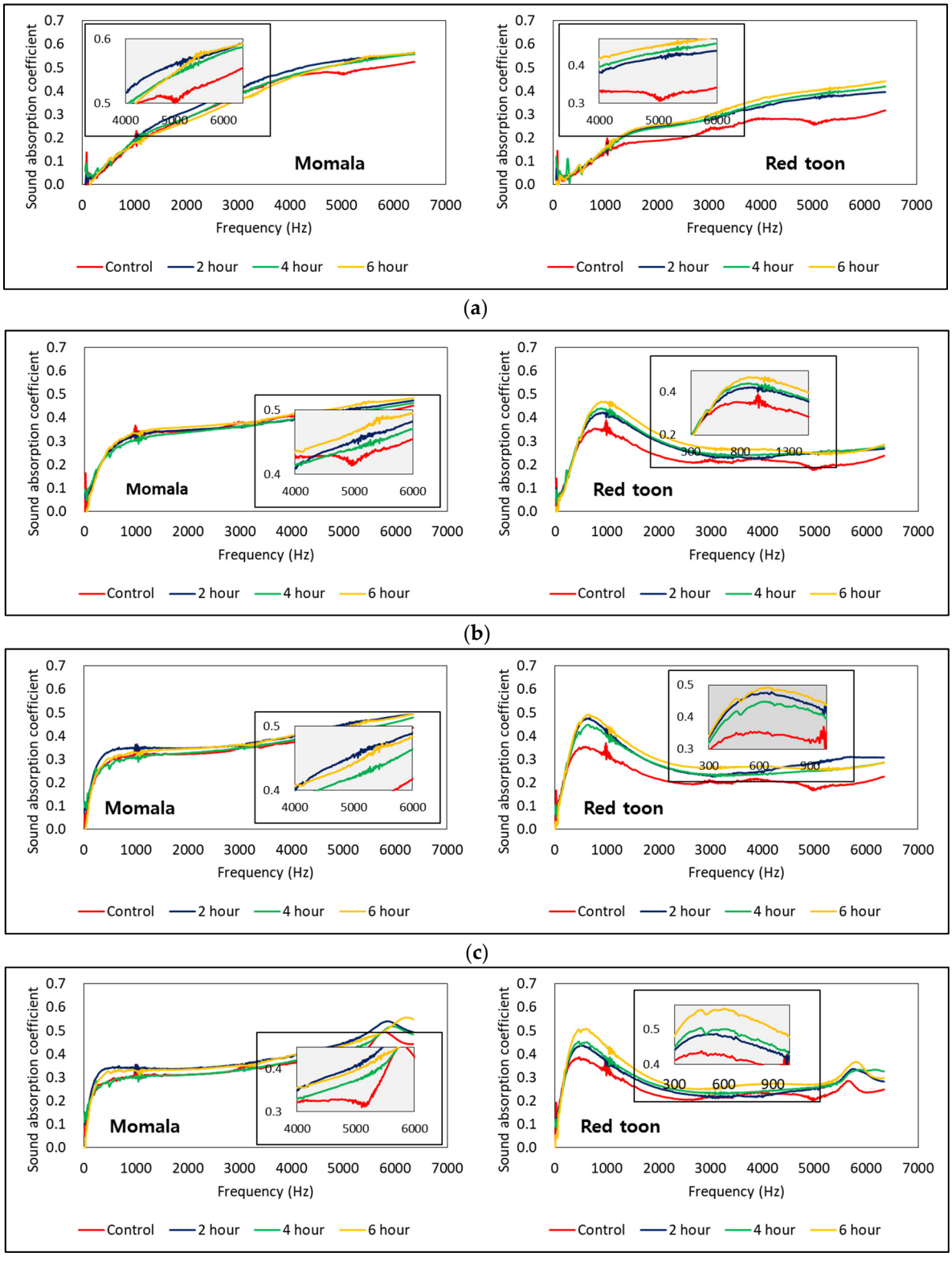

Figure 6. Alterations in sound absorption curves according to heat treatment time of momala and red toon with air back cavities of different sizes. (**a**) 1-cm air back cavity; (**b**) 2-cm air back cavity; (**c**) 3-cm air back cavity; (**d**) 4-cm air back cavity.

Table 2. NRC and sound absorption coefficient at each frequency range of momala and red toon according to heat treatment time with various air back cavity sizes.

Heat Treatment Time	Air Cavity (cm)	Momala					Red Toon				
		NRC	$\alpha_{250–500}$	$\alpha_{500–1000}$	$\alpha_{1000–2000}$	$\alpha_{2000–6400}$	NRC	$\alpha_{250–500}$	$\alpha_{500–1000}$	$\alpha_{1000–2000}$	$\alpha_{2000–6400}$
Control	None	0.147 (0.005)	0.056 (0.004)	0.129 (0.004)	0.234 (0.012)	0.439 (0.024)	0.107 (0.004)	0.042 (0.002)	0.099 (0.004)	0.175 (0.012)	0.259 (0.022)
	1	0.266 (0.019)	0.200 (0.010)	0.294 (0.033)	0.338 (0.032)	0.396 (0.021)	0.251 (0.019)	0.207 (0.007)	0.336 (0.037)	0.295 (0.034)	0.212 (0.018)
	2	0.282 (0.014)	0.256 (0.015)	0.304 (0.020)	0.323 (0.017)	0.366 (0.015)	0.281 (0.025)	0.299 (0.024)	0.342 (0.044)	0.268 (0.028)	0.200 (0.014)
	3	0.282 (0.014)	0.266 (0.013)	0.295 (0.016)	0.312 (0.015)	0.372 (0.015)	0.315 (0.027)	0.359 (0.038)	0.362 (0.041)	0.275 (0.024)	0.228 (0.020)
2 h	None	0.159 (0.009)	0.062 (0.007)	0.138 (0.005)	0.261 (0.031)	0.474 (0.028)	0.127 (0.005)	0.052 (0.002)	0.107 (0.003)	0.214 (0.012)	0.332 (0.025)
	1	0.266 (0.013)	0.201 (0.005)	0.292 (0.022)	0.338 (0.024)	0.403 (0.017)	0.285 (0.017)	0.208 (0.017)	0.383 (0.027)	0.363 (0.045)	0.249 (0.019)
	2	0.318 (0.026)	0.298 (0.035)	0.343 (0.035)	0.348 (0.002)	0.412 (0.022)	0.346 (0.040)	0.349 (0.029)	0.459 (0.088)	0.344 (0.053)	0.267 (0.043)
	3	0.326 (0.021)	0.321 (0.026)	0.342 (0.028)	0.338 (0.020)	0.416 (0.019)	0.347 (0.039)	0.393 (0.044)	0.415 (0.063)	0.310 (0.035)	0.250 (0.024)
4 h	None	0.155 (0.006)	0.072 (0.007)	0.139 (0.004)	0.242 (0.022)	0.456 (0.018)	0.130 (0.008)	0.057 (0.002)	0.105 (0.008)	0.210 (0.018)	0.342 (0.030)
	1	0.261 (0.011)	0.205 (0.008)	0.276 (0.014)	0.324 (0.016)	0.397 (0.011)	0.296 (0.013)	0.216 (0.012)	0.398 (0.023)	0.373 (0.031)	0.256 (0.015)
	2	0.284 (0.013)	0.257 (0.011)	0.293 (0.016)	0.319 (0.016)	0.390 (0.011)	0.334 (0.027)	0.337 (0.017)	0.431 (0.053)	0.339 (0.035)	0.250 (0.021)
	3	0.283 (0.021)	0.267 (0.026)	0.291 (0.027)	0.307 (0.018)	0.388 (0.013)	0.355 (0.032)	0.404 (0.038)	0.431 (0.054)	0.323 (0.032)	0.262 (0.026)
6 h	None	0.157 (0.012)	0.071 (0.006)	0.139 (0.005)	0.252 (0.038)	0.461 (0.018)	0.131 (0.054)	0.054 (0.003)	0.108 (0.006)	0.221 (0.021)	0.359 (0.027)
	1	0.271 (0.023)	0.199 (0.012)	0.303 (0.037)	0.350 (0.037)	0.418 (0.024)	0.304 (0.015)	0.204 (0.010)	0.412 (0.023)	0.406 (0.035)	0.268 (0.015)
	2	0.298 (0.020)	0.264 (0.032)	0.316 (0.020)	0.338 (0.019)	0.408 (0.016)	0.363 (0.036)	0.356 (0.014)	0.474 (0.065)	0.368 (0.050)	0.268 (0.036)
	3	0.311 (0.024)	0.295 (0.032)	0.328 (0.031)	0.332 (0.019)	0.411 (0.017)	0.392 (0.025)	0.437 (0.029)	0.486 (0.042)	0.355 (0.026)	0.279 (0.022)

The red toon sound absorption curves showed that the sound absorption coefficient was low in the low-frequency band and increased as the frequency increased. When an air cavity was applied, however, a peak occurred in the low-frequency band; this had not happened with the momala. The red toon large vessels are arranged in spring wood, act as holes, and showed resonant absorption in the rear space.

The red toon sound absorption coefficient increased as heat treatment time increased. The rate of the average sound absorption coefficient at 2000–6400 Hz increased by 38.6% ($t = -19.5301$, $p < 0.001$) during 6 h of heat treatment. The heat treatment changed the pore structure and improved the through-pore porosity, causing an increase in gas permeability that was confirmed by the improved average sound absorption coefficient at 2000–6400 Hz. This phenomenon was identical to that in momala.

The NRC of untreated red toon was 0.107 ± 0.004, and after heat treatment for 6 h, it increased by 22.4% to 0.131 ± 0.008 ($t = -11.463$, $p < 0.001$). When a 3-cm air cavity was applied, the NRC increased by approximately 190.7% to 0.311 ($t = -38.660$, $p < 0.001$) compared with untreated red toon without an air back cavity.

Table 3 shows the results of multiple regression analysis with NRC as the dependent variable and heat treatment times and air back cavities as independent variables. The F-value of the entire multiple regression model exhibited a 1% significance level, indicating that the estimated regression results were significant. Additionally, the VIF (variance inflation factor) was less than 10, which means that there was no problem with multi-collinearity [31]. The R^2 was 71.1%, which indicated that all independent variables well explained the regression models.

Table 3. Results of multi-regression analysis with NRC as the dependent variable.

$Y = \alpha_0 + \beta_1 X_1 + \beta_2 X_2 + \beta_3 D_1 + \varepsilon$				
Variables	**Coeff.**	**Std. Coeff.**	***t*-Statistic**	**VIF ***
α_0	0.149	-	25.665 **	
X_1	0.001	0.140	4.666 **	1.000
X_2	0.060	0.825	27.406 **	1.000
D_1	0.019	0.115	3.826 **	1.000
Adj. R^2	0.711			
F-value	262.505			
p-value	<0.001			

Notes: * Variance inflation factor; ** represents significance at the 1% level. Y, NRC; X_1, treatment time; X_2, air back cavity distance; D_1, wood dummy variable (1 if the wood is red toon, otherwise 0); α_0, constant (intercept term); and ε, residual (error term).

Treatment time (β_1) and presence of an air back cavity (β_2) were significant in the positive (+) direction at the 1% significance level. This indicates a statistical significance since the heat treatment time and air back cavity distance affected the improvement of sound absorption performance. The dummy variable (D_1) appeared in a positive (+) direction, which means that the improvement in sound absorption performance increased more in red toon than in momala.

3.5. What Could Be the Potential Applications for Heat-Treated Indonesian Momola and Korean Red Toon Cross Section in Construction?

This study used only the normal incidence absorption coefficient. Further analysis will be possible if cross-sectional hardwood boards are manufactured and the sound absorption coefficient values are investigated by the reverberation chamber method. In general, the random incidence absorption coefficient is higher than the normal incidence absorption coefficient in the low-frequency band [52]. Finally, we assume that the actual sound absorption performance can improve beyond this study's results.

In terms of design, Park et al. [53] proposed the cross sectional wooden wall using the pattern of annual rings in the cross-section of wood. This study proposes to use heat-treated Indonesia momala and Korean red toon cross sections as ceiling materials in construction, not only the walls. The ceiling materials using cross sectional wood can be fully utilize the air back cavity and can be maximize the sound absorption effect.

4. Conclusions

This study investigated hardwood cross sections as an eco-friendly, sustainable sound-absorbing material by improving their pore structure. To improve the gas permeability and sound absorption performance of momala and red toon cross sections, various heat treatment times and different-sized air back cavities were used. As heat treatment time increased, pore size and through-pore porosity of the wood samples increased, which improved both gas permeability and sound absorption performance. Applying an air back cavity also increased the sound absorption performance of both wood species. So, we suggest using heat-treated Indonesia momala and Korean red toon cross sections as sound-absorbing functional ceiling materials.

The results of this study are not limited to providing an efficient method for improving hardwood sound absorption performance. They also can be utilized in developing an efficient drying method that improves hardwood pore structure and an effective impregnation method for functional chemicals, including preservatives and flame retardants.

Author Contributions: E.-S.J. is the first author and designed the study, conducted all experiments, and was the major contributor to original writing, reviewing, and editing of the manuscript. C.-W.K. is the corresponding author and supervised the project and contributed to manuscript review and editing. All authors have read and agreed to the published version of the manuscript.

Funding: NRF-2019R1I1A3A02059471 and NRF-2020K2A9A2A08000181.

Institutional Review Board Statement: Not applicable.

Informed Consent Statement: Not applicable.

Data Availability Statement: Not applicable.

Acknowledgments: This research was supported by the Basic Science Research Program through the National Research Foundation of Korea (NRF) funded by the Ministry of Education (NRF-2019R1I1A3A02059471) and was supported under the framework of an international cooperation program managed by the NRF of Korea (NRF-2020K2A9A2A08000181). The authors are also thankful to the Business Startup Incubator Support Program supported by the Ministry of Education and the NRF.

Conflicts of Interest: The authors declare that they have no competing interests.

References

1. Stokholm, Z.A.; Hansen, Å.M.; Grynderup, M.B.; Bonde, J.P.; Christensen, K.L.; Frederiksen, T.W.; Lund, S.P.; Vestergaard, J.M.; Kolstad, H.A. Recent and long-term occupational noise exposure and salivary cortisol level. *Psychoneuroendocrinology* **2014**, *39*, 21–32. [CrossRef] [PubMed]
2. Green, A.; Jones, A.D.; Sun, K.; Neitzel, R.L. The association between noise, cortisol and heart rate in a small-scale gold mining community—A pilot study. *Int. J. Environ. Res. Public Health* **2015**, *12*, 9952–9966. [CrossRef]
3. Davies, H.; Van Kamp, I. Noise and cardiovascular disease: A review of the literature 2008–2011. *Noise Health* **2012**, *14*, 287. [CrossRef]
4. Raj, M.; Fatima, S.; Tandon, N. Effects of the features of a green sound-absorbing material on its acoustical properties. *Green Mater.* **2020**, *9*, 11–20. [CrossRef]
5. Mohanty, A.; Fatima, S. Noise control using green materials. *Sound Vib.* **2015**, *49*, 13–15.
6. Kang, C.-W.; Kim, M.K.; Jang, E.-S. An Experimental Study on the Performance of Corrugated Cardboard as a Sustainable Sound-Absorbing and Insulating Material. *Sustainability* **2021**, *13*, 5546. [CrossRef]
7. Asdrubali, F.; Schiavoni, S.; Horoshenkov, K. A review of sustainable materials for acoustic applications. *Build. Acoust.* **2012**, *19*, 283–311. [CrossRef]
8. KOSIS. The World Log Production. Available online: https://kosis.kr/statHtml/statHtml.do?orgId=101&tblId=DT_2KAA417 (accessed on 20 June 2021).
9. Unterrainer, W. Wood: A sustainable building material? In Proceedings of the 6th Annual International Conference on Architecture and Civil Engineering (ACE 2018), Singapore, 14–15 May 2018.
10. Scalisi, F.; Sposito, C. Measure the Embodied Energy in Building Materials: An Eco-Sustainable Approach for Construction. In *Renewable Energy and Sustainable Buildings*; Springer: Cham, Switzerland, 2020; pp. 245–255.
11. Côté, W.A.; Kollmann, F.F. Principles of Wood Science and Technology. In *Solid Wood*; Springer: Berlin/Heidelberg, Germany; New York, NY, USA, 1984; pp. 55–78. [CrossRef]
12. Wassilieff, C. Sound absorption of wood-based materials. *Appl. Acoust.* **1996**, *48*, 339–356. [CrossRef]
13. Taghiyari, H.; Zolfaghari, H.; Sadeghi, M.; Esmailpour, A.; Jaffari, A. Correlation between specific gas permeability and sound absorption coefficient in solid wood. *J. Trop. For. Sci.* **2014**, *26*, 92–100.
14. Kolya, H.; Kang, C.-W. Hygrothermal treated paulownia hardwood reveals enhanced sound absorption coefficient: An effective and facile approach. *Appl. Acoust.* **2021**, *174*, 107758. [CrossRef]
15. Kang, C.-W.; Kolya, H.; Jang, E.-S.; Zhu, S.; Choi, B.-S. Steam exploded wood cell walls reveals improved gas permeability and sound absorption capability. *Appl. Acoust.* **2021**, *179*, 108049. [CrossRef]
16. Kang, C.; Lee, N. Changes of sound absorption capability and anatomical features of wood by delignification treatment. *J. Korean Wood Sci. Technol.* **2005**, *33*, 9–14. (In Korean)
17. Jang, E.-S.; Kang, C.-W. Delignification Effects on Indonesian Momala (*Homalium foetidum*) and Korean Red Toon (*Toona sinensis*) Hardwood Pore Structure and Sound Absorption Capabilities. *Materials* **2021**, *14*, 5215. [CrossRef] [PubMed]
18. Kang, C.-W.; Jang, E.-S.; Lee, N.-H.; Jang, S.-S.; Lee, M. Air permeability and sound absorption coefficient changes from ultrasonic treatment in a cross section of Malas (*Homalium foetidum*). *J. Wood Sci.* **2021**, *67*, 1–5. [CrossRef]
19. Wang, D.; Peng, L.; Zhu, G.; Fu, F.; Zhou, Y.; Song, B. Improving the sound absorption capacity of wood by microwave treatment. *BioResources* **2014**, *9*, 7504–7518. [CrossRef]
20. Kim, Y.-S. Research trend of the heat-treatment of wood for improvement of dimensional stability and resistance to biological degradation. *J. Korean Wood Sci. Technol.* **2016**, *44*, 457–476. (In Korean) [CrossRef]

21. Esteves, B.; Pereira, H. Wood modification by heat treatment: A review. *BioResources* **2009**, *4*, 370–404. [CrossRef]
22. Boonstra, M.J.; Rijsdijk, J.; Sander, C.; Kegel, E.; Tjeerdsma, B.; Militz, H.; Van Acker, J.; Stevens, M. Microstructural and physical aspects of heat treated wood. Part 1. Softwoods. *Maderas. Cienc. Y Tecnol.* **2006**, *8*, 193–208.
23. Park, Y.; Jeon, W.-S.; Yoon, S.-M.; Lee, H.-M.; Hwang, W.-J. Evaluation of Cell-Wall Microstructure and Anti-Swelling Effectiveness of Heat-Treated Larch Wood. *J. Korean Wood Sci. Technol.* **2020**, *48*, 780–790.
24. Kang, C.-W.; Li, C.; Jang, E.-S.; Jang, S.-S.; Kang, H.-Y. Changes in sound absorption capability and air permeability of Malas (*Homalium foetidum*) specimens after high temperature heat treatment. *J. Korean Wood Sci. Technol.* **2018**, *46*, 149–154.
25. Jang, E.-S.; Kang, C.-W. Changes in gas permeability and pore structure of wood under heat treating temperature conditions. *J. Wood Sci.* **2019**, *65*, 1–9. [CrossRef]
26. Tian, M.; Zhang, B.; Wu, Z.; Yu, L.; Li, L.; Xi, X. Effects of Steam Heat-Treatment on Properties of Pinus massoniana Wood and Its Bonding Performance. *J. Renew. Mater.* **2021**, *9*, 789. [CrossRef]
27. Vernois, M. Heat treatment of wood in France: State of the art. In Proceedings of the Special Seminar "Review on heat treatments of wood", Antibes, France, 9 February 2001.
28. Putra, A.; Or, K.H.; Selamat, M.Z.; Nor, M.J.M.; Hassan, M.H.; Prasetiyo, I. Sound absorption of extracted pineapple-leaf fibres. *Appl. Acoust.* **2018**, *136*, 9–15. [CrossRef]
29. Tang, X.; Zhang, X.; Zhang, H.; Zhuang, X.; Yan, X. Corn husk for noise reduction: Robust acoustic absorption and reduced thickness. *Appl. Acoust.* **2018**, *134*, 60–68. [CrossRef]
30. Prabowo, A.E.; Diharjo, K.; Prasetiyo, I. Sound Absorption Performance of Sugar Palm Trunk Fibers. In Proceedings of the E3S Web of Conferences, Bali, Indonesia, 26–28 September 2018; p. 01003.
31. Jang, E.-S.; Yuk, J.-H.; Kang, C.-W. An experimental study on change of gas permeability depending on pore structures in three species (hinoki, Douglas fir, and hemlock) of softwood. *J. Wood Sci.* **2020**, *66*, 78. [CrossRef]
32. Pfriem, A.; Zauer, M.; Wagenführ, A. Alteration of the pore structure of spruce (*Picea abies* (L.) Karst.) and maple (*Acer pseudoplatanus* L.) due to thermal treatment as determined by helium pycnometry and mercury intrusion porosimetry. *Holzforschung* **2009**, *63*, 94–98. [CrossRef]
33. Guo, L.; Cheng, H.; Chen, J.; Chen, W.; Zhao, J. Pore Structure Characterization of Oak via X-ray Computed Tomography. *BioResources* **2020**, *15*, 3053–3063.
34. Jang, E.-S.; Kang, C.-W.; Jang, S.-S. Comparison of the Mercury Intrusion Porosimerty, Capillary Flow Porometry and Gas Permeability of Eleven Species of Korean Wood. *J. Korean Wood Sci. Technol.* **2018**, *46*, 681–691.
35. ASTM F316-03. *Standard Test Methods for Pore Size Characteristics of Membrane Filters by Bubble Point and Mean Flow Pore Test*; ASTM International: West Conshohocken, PA, USA, 2019.
36. Jang, E.-S.; Kang, C.-W. Do Face Masks become Worthless after Only One Use in the COVID-19 Pandemic? *Infect. Chemother.* **2020**, *52*, 583–591. [CrossRef]
37. Jang, E.-S.; Kang, C.-W.; Kang, H.-Y.; Jang, S.-S. Sound Absorption Property of Traditional Korean Natural Wallpaper (Hanji). *J. Korean Wood Sci. Technol.* **2018**, *46*, 703–712.
38. Jang, E.-S.; Kang, C.-W.; Jang, S.-S. Pore characterization in cross section of yellow poplar (*Liriodendron tulipifera*) wood. *J. Korean Wood Sci. Technol.* **2019**, *47*, 8–20.
39. Jang, E.-S.; Kang, C.-W. Sound absorption characteristics of three species (binuang, balsa and paulownia) of low density hardwood. *Holzforschung* **2021**. [CrossRef]
40. Rouquerol, J.; Avnir, D.; Fairbridge, C.; Everett, D.; Haynes, J.; Pernicone, N.; Ramsay, J.; Sing, K.; Unger, K. Recommendations for the characterization of porous solids (Technical Report). *Pure Appl. Chem.* **1994**, *66*, 1739–1758. [CrossRef]
41. Stange, U.; Scherf-Clavel, M.; Gieseler, H. Application of gas pycnometry for the density measurement of freeze-dried products. *J. Pharm. Sci.* **2013**, *102*, 4087–4099. [CrossRef]
42. Li, Y.; Lattimer, B.Y.; Case, S.W. Measurement and modelling of thermal and physical properties of wood construction materials. *Constr. Build. Mater.* **2021**, *284*, 122780. [CrossRef]
43. Bang, S.H.; De Beauvoir, T.H.; Randall, C.A. Densification of thermodynamically unstable tin monoxide using cold sintering process. *J. Eur. Ceram. Soc.* **2019**, *39*, 1230–1236. [CrossRef]
44. ISO12154. *Determination of Density by Volumetric Displacement—Skeleton Density by Gas Pycnometry*; International Organization for Standardization (ISO): Geneva, Switzerland, 2014.
45. Kim, A.-R.; Kim, N.-H. Effect of heat treatment and particle size on the crystalline properties of wood cellulose. *J. Korean Wood Sci. Technol.* **2019**, *47*, 299–310.
46. ISO 10534-2. *Acoustics-Determination of Sound Absorption Coefficient and Impedance in Impedance Tubes-Part 2 Transfer-Function Method*; International Organization for Standardization (ISO): Geneva, Switzerland, 2001.
47. Kwon, S.H.; Chung, G. Estimation of snow damages using multiple regression model-The case of gangwon province. *J. Korean Soc. Civ. Eng.* **2017**, *37*, 61–72. [CrossRef]
48. Liu, X.; Yan, X.; Zhang, H. Effects of pore structure on sound absorption of kapok-based fiber nonwoven fabrics at low frequency. *Text. Res. J.* **2016**, *86*, 755–764. [CrossRef]
49. Kim, B.-S.; Park, J. Double resonant porous structure backed by air cavity for low frequency sound absorption improvement. *Compos. Struct.* **2018**, *183*, 545–549. [CrossRef]

50. Yang, T.; Xiong, X.; Venkataraman, M.; Mishra, R.; Novák, J.; Militký, J. Investigation on sound absorption properties of aerogel/polymer nonwovens. *J. Text. Inst.* **2019**, *110*, 196–201. [CrossRef]
51. Shen, X.; Bai, P.; Chen, L.; To, S.; Yang, F.; Zhang, X.; Yin, Q. Development of thin sound absorber by parameter optimization of multilayer compressed porous metal with rear cavity. *Appl. Acoust.* **2020**, *159*, 107071. [CrossRef]
52. Kang, H.-J.; Kim, B.-K.; Kim, S.-R. Study on Normal and Random incidence Absorption Coefficient. In Proceedings of the Acoustical Society of Korea Conference, Seoul, Korea, 7 June 2000; pp. 283–286.
53. Park, B.H.; Hong, S.H.; Jo, W.H. The Characterization and Utilization of Wood Cross Section—Focusing on Domestic Larix kaemperi Wood & Maackia amurensis Wood. *J. Digit. Des.* **2014**, *14*, 107–116. (In Korean)